Thermal Science and Engineering Progress 50 (2024) 102512

Contents lists available at ScienceDirect

Thermal Science and Engineering Progress

journal homepage: www.sciencedirect.com/journal/thermal-science-and-engineering-progress

Numerical study of polymer embedded metal hydride-based self-sensing actuator

V. Keshav , G. Mohan *

Center for Computational Research in Clean Energy Technologies, Sree Chitra Thirunal College of Engineering, Thiruvananthapuram, Kerala, India

ARTICLE INFO

Keywords:
Soft composite actuator
Metal hydride
$LaNi_5$
Si rubber

ABSTRACT

Metal hydride actuators have amassed increasing attention over the past decade owing to their desirable operational characteristics, such as a high power-to-weight ratio, noiseless and vibration-less operation, lightweight, safety and environmental friendliness. Essentially, there are two ways in which we can attain actuation using hydrides. Primarily, actuation force is generated by the hydrogen gas pressure changes associated with charge–discharge process. Alternatively, the incompressible volumetric changes in the hydride bed during sorption can also result in actuation. However the studies reported on this type of actuators are rare and mostly deal with bimorph actuators. The present study investigates the effect of soft silicone rubber composited metal hydride bed within a hollow stainless steel spring for its potential use as a self-sensing actuator element. $LaNi_5$ is used as the metal hydride alloy. For an equivalent quantity of hydride by mass, the estimated actuation stroke and force for the composite bed actuator are better than their powder bed counterpart (12 mm and 100 N, respectively, in contrast to 5.84 mm and 60 N), due to improved heat transfer. Bed thickness, coil pitch and coil diameter are important geometric parameters which control the performance of the device. As previously reported, hydrogen supply pressure and heat transfer coefficient are found to be important operating parameters controlling the force –stroke characteristics of the actuating element. The simulation study has been executed using COMSOL Multiphysics™ commercial code.

Introduction

Climate change has become a significant issue in the recent decades, leading to different natural disasters worldwide. It is critical that we increase the reliability on sustainable and ecofriendly technologies. Many studies have investigated the prospects of implementation of advanced technologies and materials such as nanotechnology and composites [1–6]. These innovations aim to tackle ongoing environmental and economic challenges by contributing to environmental remediation, as well as the generation and storage of renewable and clean energy. Metal hydrides hold substantial significance as high-utility materials for storage of clean hydrogen energy. Although renowned as a storage medium for hydrogen, they exhibit broad applicability across numerous practical domains. Metal hydrides can utilize low-quality heat, a critical aspect in improving dependability on renewable energy sources [7–9]. With the anticipated development of a hydrogen economy, it becomes imperative to identify and explore various tools and methodologies to maximize reliability on hydrogen.

Hydride-based actuation emerges as a pivotal area requiring comprehensive investigation. There are essentially two ways in which hydride-based actuation can be realised. Primarily, by using a suitable end effector, the hydrogen gas pressure changes during sorption process can give an actuation force. The other way is to utilise the inherent property of metal hydrides to expand and contract in volume during the hydrogen breathing process. Numerous studies have been conducted on hydrogen gas pressure-driven actuators, particularly in rehabilitative systems and biomimetic applications such as artificial muscles [7–10]. However, studies reported on such actuation, resulting from the mechanical expansion and contraction during sorption, is limited and primarily confined to bimorph actuators.

Y. Nishi *et* al. [11] investigated the behaviour of a soft bimorph actuator composed of two rubber sheets, with one sheet dispersed with $LaNi_3CO_2$ powder. Strains of 4000 ppm were induced, resulting in significant bending motion during hydrogenation lasting from 100 s to 10,800 s. M. Mizumoto *et* al. [12] explored the bending behaviour of a Cu-plated hydrogen storage alloy. Plating of a non-hydrogenation element on a hydrogenation element was implemented to convert the volume expansion of the latter into bending motion. A. Nakai *et* al. [13] analysed the parameters controlling the rotation and bending of a

* Corresponding author.
E-mail address: mohan.g.menon@sctce.ac.in (G. Mohan).

https://doi.org/10.1016/j.tsep.2024.102512
Received 29 November 2023; Received in revised form 29 February 2024; Accepted 7 March 2024
Available online 13 March 2024

Nomenclature

C_a&C_d	Material dependent constants
E_a&E_d	Activation energy
A&B	van't Hoff constants
E	Youngs modulus
V	Volume fraction
R	Universal gas constant
D_f	Diffusivity
Nu	Nusselt number
Ra	Rayleigh number
D	Coil diameter
P_t	Axial pitch
h	Convective heat transfer coefficient
H_a	Activation energy
F	Reacted fraction
n	Phani-Niyogi exponent
P	Pressure
T	Temperature
$\dot{m}$	Mass rate of H_2 sorption
C_P	Specific heat
Gr	Grashof number
Pr	Prandtl number
do	Tube outer diameter
L	Length of tube
K_B	Boltzmann constant

Greek letters

ρ	Density
ϕ	Expansion ratio
λ	Thermal conductivity
ε	Bed porosity
ΔH	Enthalpy of formation
α	Thermal expansion coefficient
μ	Dynamic viscosity
ß	Volume expansion coefficient
Ψ_{max}	Maximum filler volume fraction
Δ S	Entropy of formation

Subscripts

eq	Equilibrium
e	Effective value
b	Metal hydride bed
0	Initial value
sat	Saturated
q	Net value
c	Composite
g	Gas
p	Particle
a	Absorption
d	Desorption
f	Ambient fluid
cr	Critical value
m	Matrix

bimorph actuator made up of a Pd-Ni alloy and Cu strips. The response time and displacement of the actuator were characterized for different strip thicknesses and aspect ratios. K. Numasaki *et* al. [14] investigated the improvement in the response of a unimorph actuator made up of $LaNi_5$ film deposition on polyimide sheet, by ion sputtering of Pd. Hydride-based bimorph and unimorph actuators show appreciable displacement, but their force attribute is restricted. K. Goto *et* al. [15] investigated the deformation in a capsule-type metal hydride actuator, wherein a hollow epoxy resin capsule housed a metal hydride foil partially inserted in its inner wall. The expansion of the hydride foil during hydrogen absorption induced contraction of the capsule, allowing for linear actuation. Their stroke is in the order of micrometres range and the force is also limited. P. V. Jithu and G. Mohan [16] evaluated the efficacy of a spring-type actuator which makes use of hydride volume expansion. Their geometric configuration included $LaNi_5$ hydride alloy in the powdered form encased within a coiled tube. The selection of

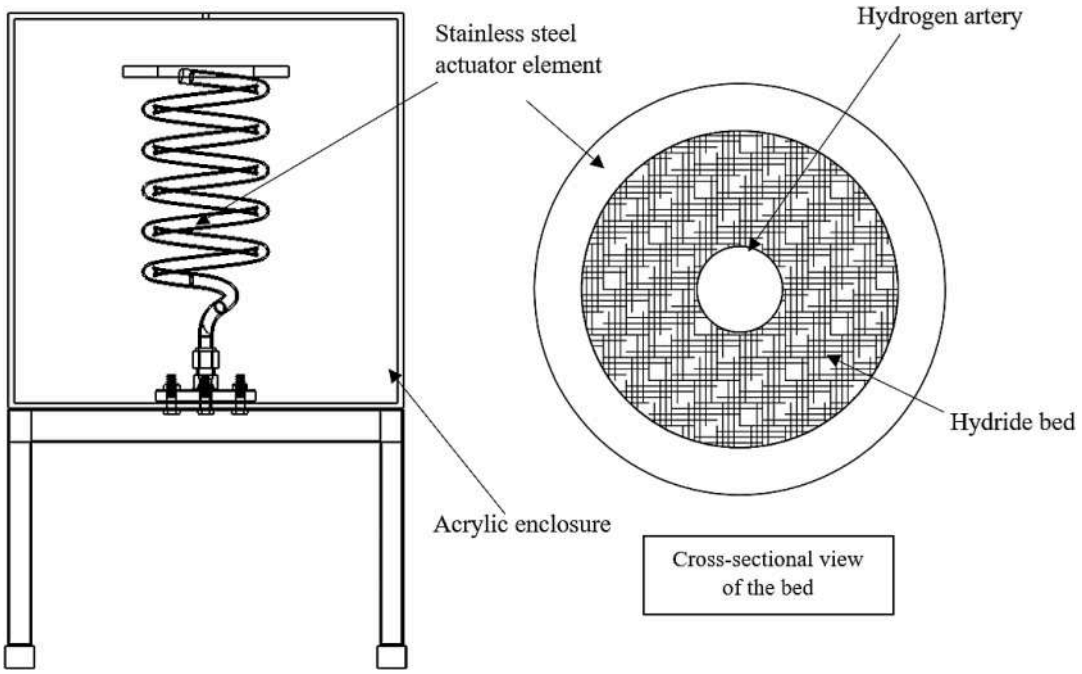

Fig. 1. Schematic of metal hydride-based spring type actuator.

geometry was adept at translating the hydride expansion and contraction, to actuation, by leveraging the elastic potential of the spring walls. Despite exhibiting better actuation characteristics compared to the previous studies, utilization of hydride in the granular form is impractical. This is because of the tendency of $LaNi_5$ to pulverize with progressive sorption cycles.

H. Uchida *et* al. [17] examined the influence of mixing $LaNi_5$ in silicone rubber, for imparting pulverization resistance to the hydride. Few other studies on such composites were investigated for improved heat transfer characteristics and dimensional stability [18,19]. R. Checchetto *et* al. [20] characterized the sorption behaviour of a $LaNi_5$-polysiloxane composite with two different weight fractions of $LaNi_5$ (83 wt% and 55 wt%). The composite with higher wt.% of hydride behaved like a metal matrix, whereas the one with lower wt.% of hydride resembled a polymer matrix. In an alternate study [21], the same authors investigated the sorption performance of $LaNi_5$ alloy embedded in polysiloxane (PS) and polyethylene (PE) in comparison with non-embedded $LaNi_5$ alloy. For PS-$LaNi_5$ composite (77 wt% of $LaNi_5$), the hydrogenation levels are found to be poor. This is attributed to the formation of interfacial bonds between the metal atoms and the functional groups of polymers, which affects the diffusivity of hydrogen throughout the matrix and reduces the amount of hydrogen accumulating the interface. This results in lower surrounding hydrogen concentration required for hydrogen reduction of the active metal sites. For PE-$LaNi_5$ (50 wt% of $LaNi_5$), quick activation and better hydrogenation levels are achieved due to their weak association with metal atoms. W. R. Schmidt [22] determined the significance of using polymer dispersed metal hydride for hydrogen storage. Such composite tailoring is done to make use of the low density of polymer with the high-volume capacity of the hydride, which improves gravimetric storage capacity of metal hydride alloys.

The bimorph actuators driven by hydride volume expansion produce less actuation force. This limitation can be addressed by choosing a more viable geometry. The study done by authors [16] using a spring configuration as hydride bed enclosure aims to address this problem. However, particle fragmentation during reversible sorption cycles can be significant, leading to gravitational settling, local densification. This causes stress accumulation during bulk expansion [23]. Hydrogenation, limited by poor heat transfer in powder bed can lead to slow response [23].

As reported in [17–22], multiple studies have employed a polymer-hydride composite for ensuring hydride structural stability in hydrogen storage applications. However, no investigation into its utilization for an actuation purpose has been reported. This study represents a novel attempt to tailor the prospects of polymer dispersed hydride composite with a convenient spring-type geometry for their possible end use as an effective actuator element. Such actuators can be utilized in soft robotics and haptic interfaces, where their responsiveness to thermal stimuli can be leveraged, enabling their use as self-sensing actuators or sensors.

Physical model

The schematic of the spring tube bed is depicted in Fig. 1. Owing to their high tensile strength and resistance to hydrogen embrittlement, AISI 316 material is considered for the spring tube enclosure. $LaNi_5$-Si rubber composite is packed within the tube. A central artery is provided to uniformly supply hydrogen gas. The entire arrangement is then coiled to a suitable coil diameter and pitch. The system is hermetically sealed to impede hydrogen leakage.

During hydriding process, hydrogen gas gets absorbed into the bed in an exothermic reaction. The stainless steel enclosure dissipates the generated heat from the bed to the surrounding air. The absorption will cause the bed to expand in volume. The force exerted by this incompressible expansion will cause the spring to uncoil, yielding a stroke. The limit of expansion is reached when the bed gets completely saturated with hydrogen. Consequently, the maximum actuation stroke corresponds to the hydrogen saturation point in the bed.

Following assumptions are adopted to simplify the numerical model.

a. The polymer-hydride composite is considered isotropic.
b. The hydriding alloy is presumed to possess negligible plateau slope and hysteresis.
c. The association of the hydride and polymer is assumed not to alter the hydrogen storage capacity of the alloy.
d. The dispersed alloy particles are treated as spherical.
e. The pressure drop across the bed thickness is considered negligible.
f. The gas diffusion resistance offered by the polymer is neglected.
g. Convection and conduction are deemed the primary heat transfer modes, while radiation effects are negligible.
h. The inertial effects of the spring are disregarded.

Problem formulation

Mass balance

Hydrogen gas is supplied to the bed through the porous filter. The mass transport of hydrogen within the hydride bed driven by concentration gradient is represented using the following equation:

$$(1-\varepsilon)\frac{\partial \rho_b}{\partial t} = \dot{m} + (1-\varepsilon)\frac{\partial}{\partial x}\left(D_f \frac{\partial \rho_b}{\partial x}\right) + (1-\varepsilon)\frac{\partial}{\partial y}\left(D_f \frac{\partial \rho_b}{\partial y}\right) \quad (1)$$

LHS gives the rate of change of mass of the hydride bed. The first term in RHS gives the mass flow rate of hydrogen gas and the second and third terms represents the diffusive transport due to concentration gradient in the bed. The potential of the gas to diffuse into the sorbent medium is given using the diffusivity relation.

$$D_f = D_{f_0}\exp\left(\frac{-H_a}{K_B T}\right) \quad (2)$$

Energy balance

Depending on whether the process is absorption or desorption, heat gets released or absorbed. Heat conduction transport across the hydride bed is represented using the equation:

$$(\rho C_P)_e \frac{\partial T}{\partial x} = \lambda_e \left[\frac{\partial}{\partial x}\left(\frac{\partial T}{\partial x}\right) + \frac{\partial}{\partial y}\left(\frac{\partial T}{\partial y}\right)\right] - \dot{m}\Delta H \quad (3)$$

The first term in the RHS accounts the heat conducted across the bed and the second term represents the heat absorbed or desorbed by the bed respectively during dehydrogenation and hydrogenation. The polymer embedded with hydride alloy is a case of particle dispersed composite with the metal hydride being the dispersed particles. For convenience and to avoid the complex formulations, the hydride particles are assumed to be spherical. Among the classical models, the Lewis-Nielsen model gives appreciable results for the effective thermal conductivity of particle dispersed composites with moderate filler fractions up to 40 % [24].

$$\frac{\lambda c}{\lambda m} = \frac{1+QWVp}{1-W\varphi Vp}\quad W = \frac{\frac{\lambda}{\lambda_m}-1}{\frac{\lambda}{\lambda_m}+Q}\quad \varphi = 1+\left(\frac{1-\Psi_{max}}{\Psi_{max}^{\ 2}}\right)V_P \quad Q = 1.5 \text{ for spherical particles} \quad (4)$$

Reaction kinetics

The sorption kinetics equations are given as follows:

$$Absorption rate: \quad \dot{m} = C_a \exp\left(\frac{-E_a}{RT}\right)\ln\left(\frac{P}{Peq}\right)\cdot(\rho_{sat}-\rho_b) \quad (5)$$

$$Desorption rate: \quad \dot{m} = C_d \exp\left(\frac{-E_d}{RT}\right)\ln\left(\frac{P-Peq}{Peq}\right)\cdot(\rho_b) \quad (6)$$

These are semi-empirical relations that govern the absorption and desorption of metal-hydride. The equilibrium pressure is determined as from van't Hoff plot:

$$\ln P_{eq} = A - \frac{B}{T} \tag{7}$$

This equation controls the behaviour of the hydride at the plateau region. A hydrogen gas supply pressure above this pressure starts hydrogenation and when the supply pressure is below this value, dehydrogenation occurs.

Variation in porosity

The change in porosity of the reactor bed due to bed particle expansion and contraction is given by [25]:

$$\varepsilon = 1 - (1 - \varepsilon_0)\frac{1 + \phi_p F}{1 + \phi_b} \tag{8}$$

Porosity input is a record of the packing rate or the mass of the metal assembled in a bed. The variation in porosity during hydriding/dehydriding process is minor and their effect on the bed properties is insignificant. During sorption, the particles bulge out or shrink making differential area contact eventually causing slight modifications to the bed thermal conductivity and heat capacity. These considerations during theoretical analysis will give a more accurate approximation of the expansion–contraction behaviour of the metal hydride bed. However, in the practical scenario, porosity is not a controllable parameter. Furthermore, the volume expansion induced alterations in porosity are negligible.

Convective heat transfer coefficient

For vertical helicoid tube, the convective heat transfer coefficient is obtained from the set of relations given in [26]. For natural convection, the fluid molecules that get heated, due to their relative low density rises up and the low temperature molecules descend. Density variation is therefore the driving force for free convection. From the following expressions, the convective heat transfer coefficient can be determined.

$$H = \frac{Nu\lambda}{d_0} \quad Nu = 0.0779(Ra)^{0.275}\left(\frac{D}{do}\right)^{0.184}\left(\frac{P_t}{do}\right)^{0.212}\left(\frac{L}{do}\right)^{0.108} \tag{9}$$

$$Gr = \frac{\rho^2 \beta g \Delta T L^3}{\mu^2} \quad Pr = \frac{C_P \mu}{\lambda} \quad Ra = GrPr$$

Structural mechanics equations

Properties of $LaNi_5$ is taken as the properties for the particle and that of Silicone rubber is considered for properties of the matrix in the empirical relations used to determine the effective values of the composite bed.

Effective Youngs modulus

Considering the effect of bed porosity, the effective elastic modulus is given by Phani-Niyogi equation [27]:

$$E_e = E_q\left(1 - \frac{\varepsilon}{\varepsilon_{cr}}\right)^n \tag{10}$$

Here, ε_{cr} is the critical porosity at which the neighbouring particles does not make any contact. The net mechanical properties of a two-phase composite can be obtained from the law of mixtures which considers that each component phases contribute to the effective property regarding their volume fractions. This model assumes that mixture constituents experience the same strain.

Table 1
Physical properties of $LaNi_5$, Si rubber & AISI 316 used for simulation [16,28,30].

	$LaNi_5$	Hydrogen	AISI 316	Si rubber
Activation energy for absorption (Ea) [J mol^{-1}]	21,170	–	–	–
Specific heat (Cp) [J kg^{-1} K^{-1}]	419	14.890	468	1050
Density [kg m^{-3}]	8200	0.0838	8000	1100
Reaction kinetics constant (Ca) [s^{-1}]	59.187	–	–	–
Van't Hoff constant (A)	12.99	–	–	–
Van't Hoff constant (B)	3704.59	–	–	–
Effective thermal conductivity of bed [W/m.K]	0.75	0.1825	13.6	0.3993
Thermal expansion coefficient [mm^{-1} K^{-1}]	1.23e-5	–	1.8e-5	250e-6
Modulus of elasticity [GPa]	140	–	204	0.001
Poisson's ratio	0.31	–	0.3	0.47

$$E_q = E_p V_p + E_m V_m \tag{11}$$

Expansion coefficient

The following relation gives the coefficient of expansion of the hydride bed accounting both thermal and volumetric expansion of the hydride, that vary linearly with bed temperature [28].

$$\alpha_e = \alpha\left[1 + \alpha\Delta T + \frac{\phi_b}{3\alpha\Delta T}F\right] \tag{12}$$

The factors governing the coefficient of thermal expansion of a particle dispersed composite are the particle shape, size, distribution, and volume fraction, and also the interfacial characteristics of the matrix and dispersion or between the dispersed particles for the case of higher particular concentrations. Turner's modification [29] to Voigt model gives the effective thermal expansion for composites as follows:

$$\alpha = \frac{V_p E_p \alpha_p + V_m E_m \alpha_m}{V_p E_p + V_m E_m} \tag{13}$$

Initial and boundary condition

The initial temperature and pressure of spring bed is assumed to be a constant.

$$\rho_{b_0} = \rho_b; \quad P = P_0; \quad T = T_0 \tag{14}$$

The entire spring bed is leakage proof and hydrogen gas is supplied at a constant pressure to the reactor bed. The heat transfer to and from the spring bed manifests through the heat flux at the outer surface of the spring walls. The heat transfer coefficient consideration is based on free convection. Hydrogen is supplied through a porous artery insert concentric to the spring bed. Therefore, the boundary between the bed and the artery is permeable to hydrogen gas transfer as well as heat transfer. The boundary conditions are therefore as follows:

- *At the spring wall*:

$$\partial\rho = 0; \quad \partial P = 0; \quad -\lambda_e \partial T = h_f(T_f - T) \text{ at } t > 0 \tag{15}$$

- *At the porous filter tube wall:*

$$\partial\rho_b = 0; \quad P = P_0; \quad \partial T = h_g(T_g - T) \text{ at } t > 0 \tag{16}$$

- The base end of the spring is fixed, and the spring is constrained to undergo motion only in the axial direction.

Table 2
Parametric ranges used for the simulation.

No. of coils	8.32 (5 for granular bed)
Stainless-steel tube diameter	12.7 mm
Stainless-steel tube thickness	1.65 mm
Hydride bed thickness	3 mm
Hydrogen filter diameter	3 mm
Axial pitch of the spring arrangement	36 mm
Mean diameter of the spring	100 mm
Total weight of hydride	0.4056 kg
Constant bed pressure (bar)	5
Initial bed temperature (K)	295
Initial bed concentration (mol/m^3)	18981.48
Surrounding air temperature (K)	295
Convective heat transfer coefficient (W/m^2 K)	22–27

Simulation methodology

The simulation study is done using COMSOL Multiphysics™ commercial code. The primitive models from the geometry tab were used to model three distinct domains which include the composite bed, stainless steel enclosure and the hydrogen supply artery. The entire geometry is discretized into tetrahedral and prism elements using suitable mesh parameters availed in the software. Grid independence has been established. The materials were either chosen from the library or generated as a blank material allocating the properties outlined in Table 1. They were then subsequently assigned to the corresponding domains. The equations governing various physics of the problem are integrated to the corresponding domains using inbuilt features in the software. Three application modules are used for the simulation study. 'Transport of diluted species in porous media' is used to simulate the sorption process in the composite bed. 'Heat transfer in porous media' is used to simulate the heat transfer due to convection occurring at the exterior surface of the enclosure, the conduction of heat between the spring wall and the composite bed, and the heat transport within the bed. 'Solid mechanics' module is used to simulate the structural mechanics of the system like thermal expansion, volume expansion, force, and stroke. Boundary and initial conditions are provided as necessary. The initial values used for essential parameters are given in Table 2. By employing the 'Parametric Sweep' module, simulations were carried out for various hydrogen gas supply pressure, convective heat transfer coefficient on the enclosure surface and bed thickness to understand their influence on sorption process of the bed and consequently the spring actuation. Additionally, the module was used for investigating the effect of different axial pitches and coil diameters on the spring actuation.

Validation

The validation of the adopted physics modules was done with reference to the experimental studies done in [18]. Si rubber and $LaNi_5$ mixed in the ratio of 40/1 wt ratio, is coated over a brass tube which is subsequently sealed in a larger tube. Water flowing through the brass tube provides heat transfer. Hydrogen gas is supplied to the concentric tube enclosing the coated brass tube and the hydrogen sorption process in the coating is studied. The schematic of the setup is given in Fig. 2. An average deviation of 5.54 % is observed.

Results and discussion

The simulations are performed for $LaNi_5$ as the metal hydride and Si rubber as the polymer. $LaNi_5$ has rapid and reversible sorption kinetics. The sorption in $LaNi_5$ is thermally well controlled. This alloy is thoroughly characterized and its thermo-physical properties are well established in literature. This is given in Table 1. Swelling as high as 25 % is achieved for these alloys during hydrogen breathing. Si rubber does not react chemically with hydrogen and it offers less restriction for hydrogen percolation.

The primary goal of this work is to carry out a numerical investigation into the functionality of soft hydride-based composite actuator. The performance of the composite actuator is compared with the actuator encasing $LaNi_5$ alloy without embedding Si rubber. The geometric characteristics of the spring enclosure and the parametric ranges used for the simulation, are outlined in Table 2. It must be acknowledged that, to accommodate an equivalent mass of $LaNi_5$ as in the granular bed, the volume required for the composite bed exceeds that of the

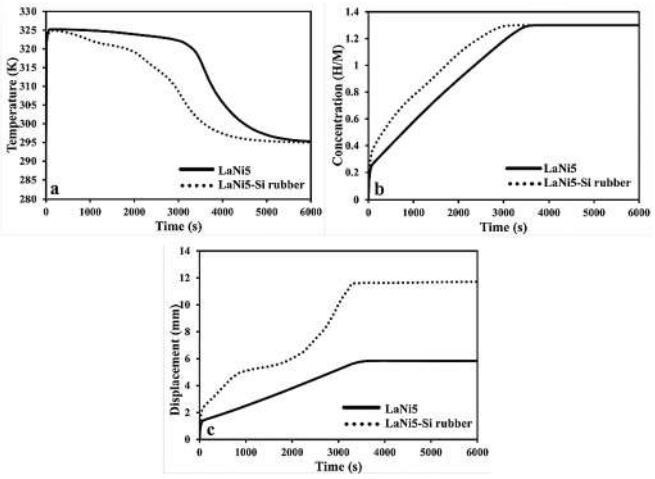

Fig. 3. Variation of a) average bed temperature b) average bed concentration c) Actuation stroke of $LaNi_5$ powder and $LaNi_5$-Si rubber composite beds (T_o = 295 K, P_o = 5 bar, h = 22 W/m^2 K, Bed thickness = 3 mm, Axial Pitch = 36 mm, Spring constant = 7.874, Coils = 5($LaNi_5$) 8.32 ($LaNi_5$-Si)).

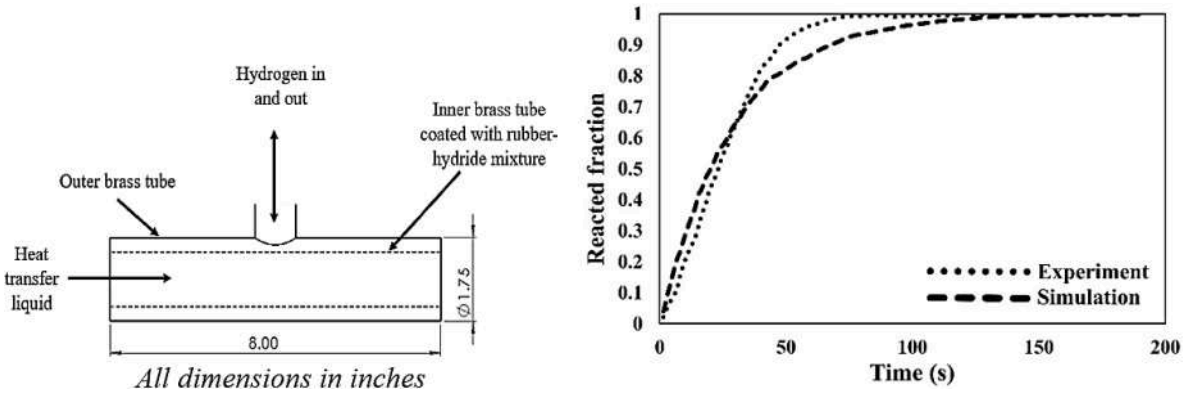

Fig. 2. Validation of hydriding simulation results with experimental data [18].

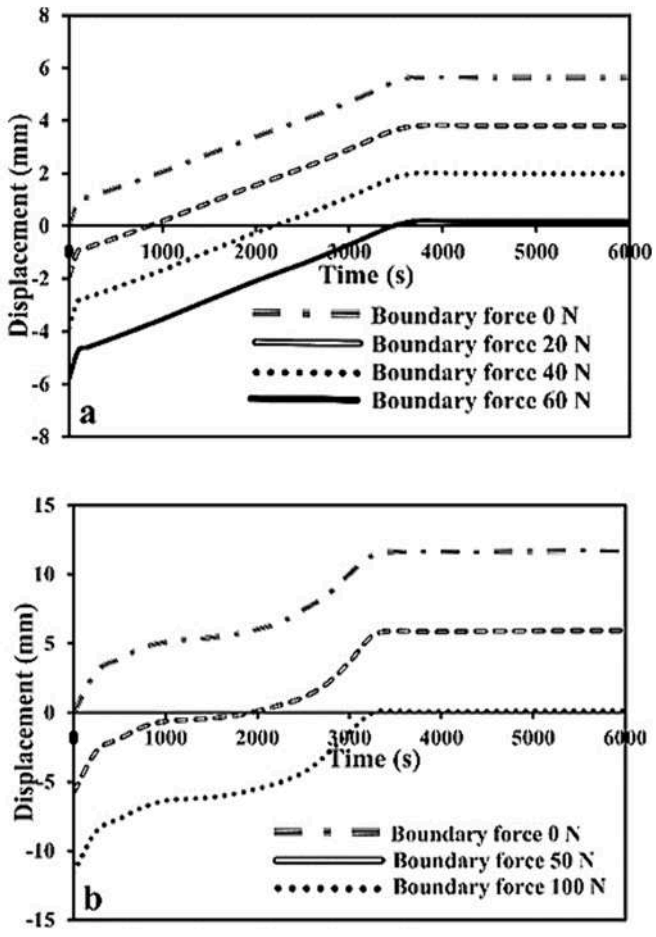

Fig. 4. Variation of actuator stroke in a) $LaNi_5$ powder and b) $LaNi_5$-Si rubber composite beds when subjected to different loads (T_o = 295 K, P_o = 5 bar, h = 22 W/m^2 K, Bed thickness = 3 mm, Axial Pitch = 36 mm, Spring constant = 7.874, Coils = 5($LaNi_5$) 8.32 ($LaNi_5$-Si)).

granular bed. This difference is equilibrated by employing 8.32 turns for the composite actuator, as opposed to the 5 turns for the powder bed actuator. The minimum coil diameter of 100 mm is mandated to coil an AISI 316 tube with a maximum wall thickness of 1.65 mm without any distortions. $LaNi_5$ considered for the simulation amounts to 84 wt% in the composite. This would render an effect similar to particle dominant composite as studied in [20]. For this case the alterations in the hydrogen storage capacity of the hydride due to polymer association can be neglected and the polymer serves as a binder only.

Fig. 3 compares the variation of the average bed temperature, concentration, and actuator stroke during hydrogenation between the composite bed and the granular bed. At the onset of absorption itself, the bed temperature suddenly shoots up, depicting the exothermic nature of hydriding process. It is evident from Fig. 3(a) that the heat transfer rates in the composite bed is substantially more than the powder bed. This is a consequence of the lower thermal conductive resistance due to interfacial line contact between adjacent hydride particles. This ensures good heat transfer within the bed as well as between the enclosure wall and bed. It is clear from the hydrogen concentration plot that during the initial stages, only a modicum of the total storage capacity got absorbed. This phase is governed by the material properties and occurs rapidly, as indicated by the steep initial slope of the concentration plot during hydrogenation. As the bed temperature increases, the pressure potential responsible for hydrogen breathing decreases. The influence of heat transfer brings down the bed temperature, subsequently increasing the pressure difference. The major portion of sorption process is controlled

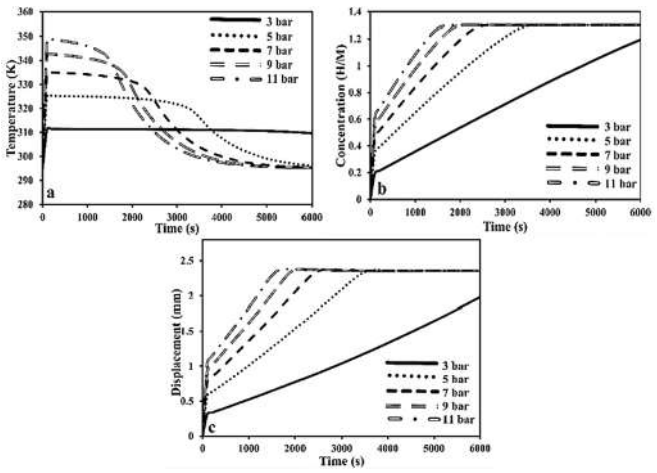

Fig. 5. Effect of H_2 supply pressure on a) Average bed temperature b) Bed concentration c) Actuator displacement during hydriding process in $LaNi_5$ granular bed (T_o = 295 K, P_o = 3–9 bar, h = 22 W/m^2 K, Bed thickness = 3 mm, Axial Pitch = 36 mm, Spring constant = 7.874, Coils = 5($LaNi_5$) 8.32 ($LaNi_5$-Si)).

by heat transfer from the bed and hence, from Fig. 3(b) it is apparent that the hydrogen absorption rate for the composite bed is quicker than the granular bed. The composite bed reaches hydrogen saturation around 3000 s whereas the granular bed takes around 3500 s to reach saturation. The contribution of convective heat transfer is maintained constant in both cases to account the changes in conduction properties alone which are direct implications of using two distinct structural media for the bed. After saturation, no further heat gets released from the bed and the effect of heat flux leads to a decrease in bed temperature. The displacement trend shown in Fig. 3(c) appears more or less self-similar to the concentration plot. This indicates that hydride volume expansion predominantly influences the actuator stroke. It clearly depicts that the actuation stroke is better for the composite bed. A maximum stroke of approximately 12 mm is observed for the composite bed in contrast to 5.84 mm for the granular bed. Certain non-linear instances can be observed in the displacement curve of the composite which can be attributed to the impact of thermal contraction of the rubber component. Si rubber has a high thermal expansivity. The nonlinear patterns observed in the displacement plot align with fluctuations in bed temperature, indicating that temperature changes are responsible for this behaviour. For both the cases, an initial stroke of 1 mm within 10–15 s is observed which can be attributed to the sorption process pertaining to the material properties of the hydriding alloy.

Fig. 4 illustrates the force characteristics of the granular and composite spring beds. As shown in Fig. 4(a), to estimate the actuation force, the spring was subjected to boundary loads ranging from 0 to 60 N, and the boundary load at which the actuation stroke is completely neutralized is considered as the required force value. Thus, the actuation force is approximated as 60 N for the powder bed case. The actuation force is evaluated in a similar manner for the composite bed. The force for complete negation of the actuator stroke is observed to be approximately 100 N.

The operational parameters relevant to the physics of metal hydride sorption like H_2 gas supply pressure, heat transfer coefficient and bed thickness were studied. Parametric studies were conducted on both the actuator types during hydrogen absorption process. The results are self-similar for both the actuators.

Figs. 5 and 6 depicts the influence of H_2 gas supply pressure on actuator performance of the respective beds. Parametric sweep was undertaken for 3, 5, 7, 9 and 11 bar pressures. It can be observed that the absorption rate increases with H_2 gas pressure, thereupon the response to maximum stroke increases with supply pressure of hydrogen. This is

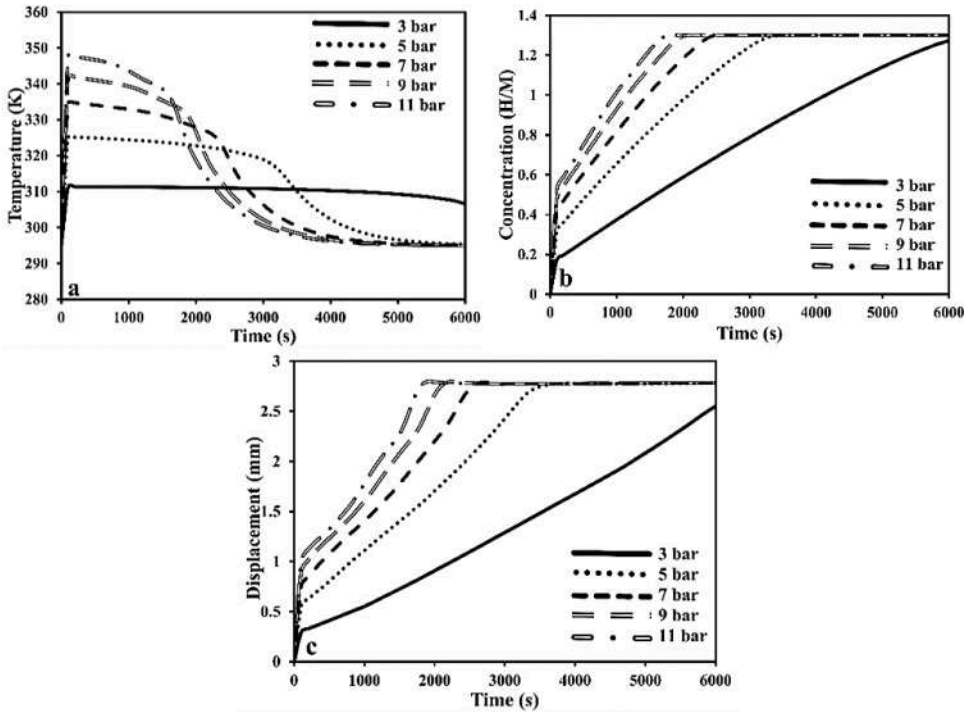

Fig. 6. Effect of H_2 supply pressure on a) Average bed temperature b) Bed concentration c) Actuator displacement during hydriding process in $LaNi_5$-Si rubber composite bed (T_o = 295 K, P_o = 3–11 bar, h = 22 W/m^2 K, Bed thickness = 3 mm, Axial Pitch = 36 mm, Spring constant = 7.874, Coils = 5($LaNi_5$) 8.32 ($LaNi_5$-Si)).

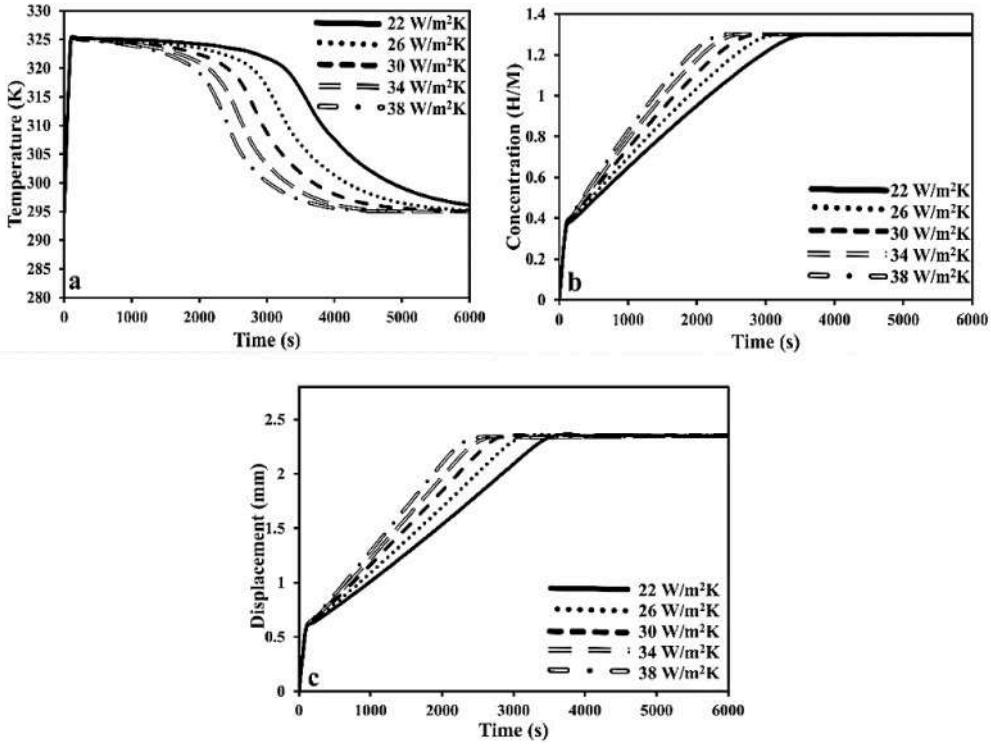

Fig. 7. Effect of heat transfer coefficient on a) Average bed temperature b) Bed concentration c) Actuator displacement during hydriding process in $LaNi_5$ granular bed (T_o = 295 K, P_o = 5 bar, h = 22–38 W/m^2 K, Bed thickness = 3 mm, Axial Pitch = 36 mm, Spring constant = 7.874, Coils = 5($LaNi_5$) 8.32 ($LaNi_5$-Si)).

because, the pressure differential between the equilibrium pressure and the supply pressure, which drives the hydrogenation process, will increase with supply pressure. The maximum temperature attained by the bed increases with supply pressure. In the absence of any heat transfer mechanism, the exothermicity induced rise in bed temperature tends the pressure differential to zero, abruptly stopping the absorption process. Increased gas pressure prolongs the absorption process, leading to more extensive heat rejection and consequently resulting in higher bed temperatures.

Figs. 7 and 8 depicts the influence of convective heat transfer

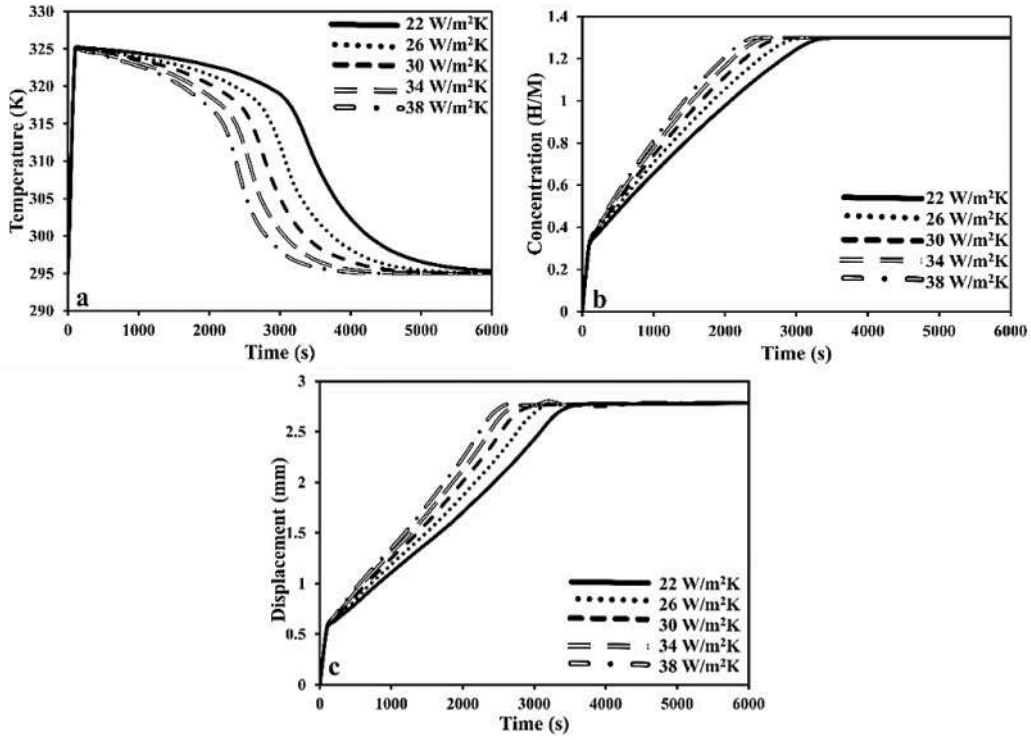

Fig. 8. Effect of heat transfer coefficient on a) Average bed temperature b) Bed concentration c) Actuator displacement during hydriding process in $LaNi_5$-Si rubber composite bed (T_o = 295 K, P_o = 5 bar, h = 22–38 W/m^2 K, Bed thickness = 3 mm, Axial Pitch = 36 mm, Spring constant = 7.874, Coils = 5($LaNi_5$) 8.32 ($LaNi_5$-Si)).

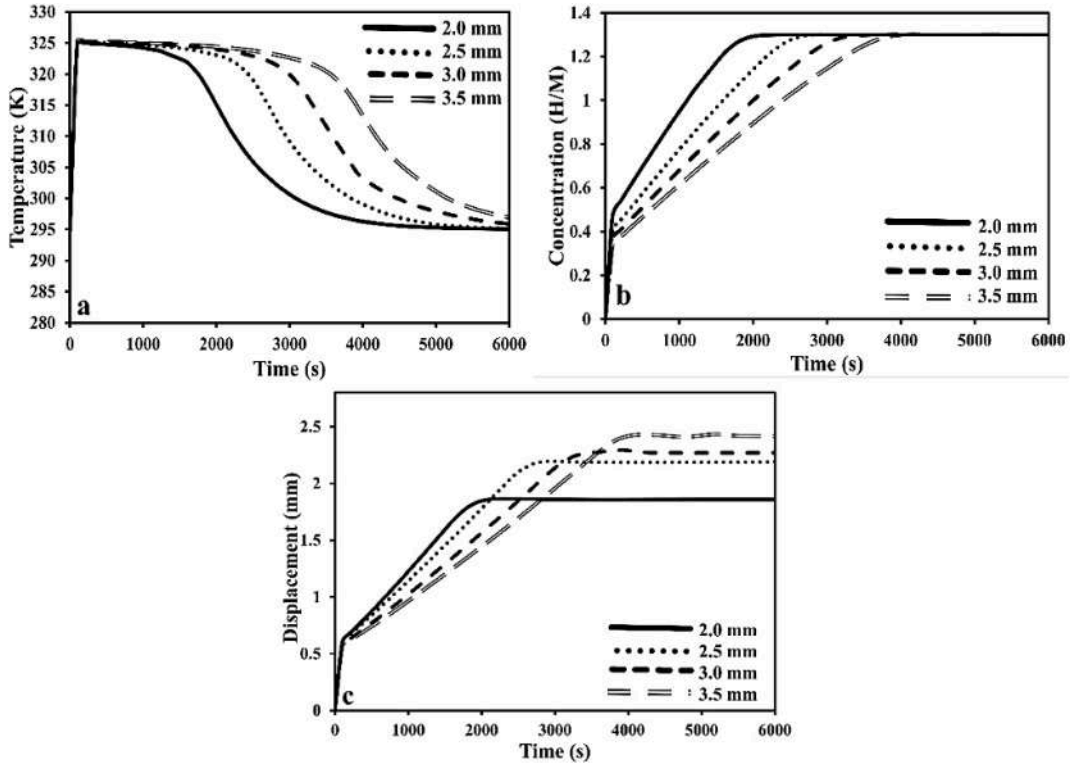

Fig. 9. Effect of bed thickness on a) Average bed temperature b) Bed concentration c) Actuator displacement during hydriding process in $LaNi_5$ granular bed (T_o = 295 K, P_o = 5 bar, h = 22 W/m^2 K, Bed thickness = 2–3.5 mm, Axial Pitch = 36 mm, Spring constant = 7.874, Coils = 5($LaNi_5$) 8.32 ($LaNi_5$-Si)).

coefficient respectively on powder and composite actuator performance. Parametric sweep conducted on convective heat transfer coefficient, the range of values taken were 22, 26, 30, 34 and 38 W/mK. The predominant phase of hydrogenation is regulated by heat transfer rates. Therefore, with increase in convective heat transfer coefficient the absorption rate increases. Quicker the heat transfer rates, the hydrogen saturation is reached quickly. Since volume swelling of the hydriding bed is a function of hydrogen absorption, the actuator displaces to its

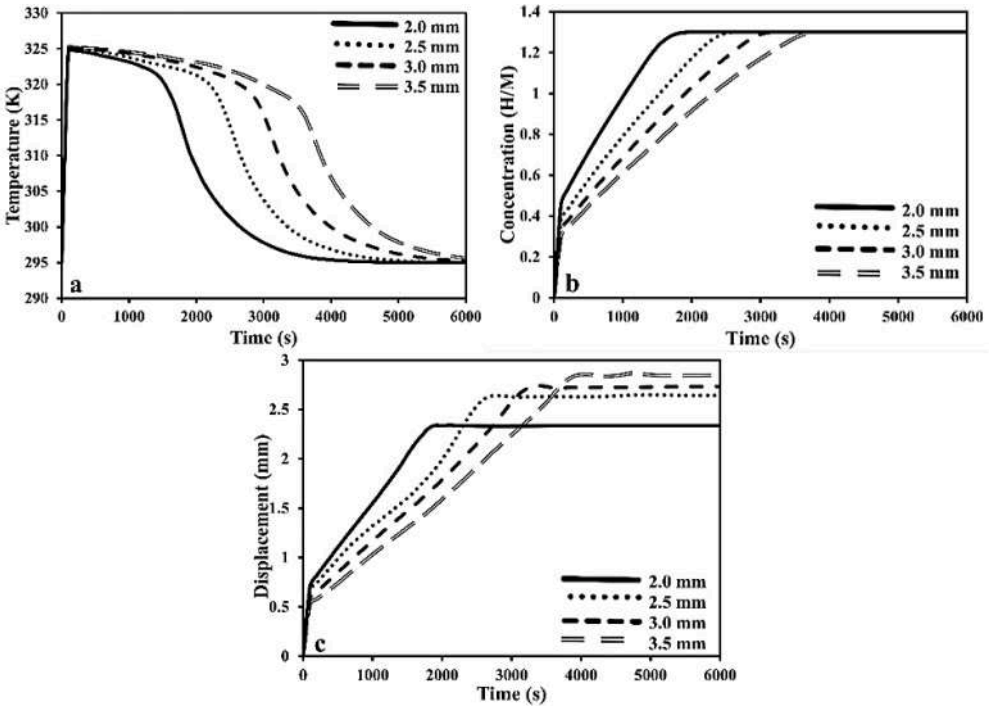

Fig. 10. Effect of bed thickness on a) Average bed temperature b) Bed concentration c) Actuator displacement during hydriding process in $LaNi_5$-Si rubber composite bed (T_o = 295 K, P_o = 5 bar, h = 22–38 W/m^2 K, Bed thickness = 2–3.5 mm, Axial Pitch = 36 mm, Spring constant = 7.874, Coils = 5($LaNi_5$) 8.32 ($LaNi_5$-Si)).

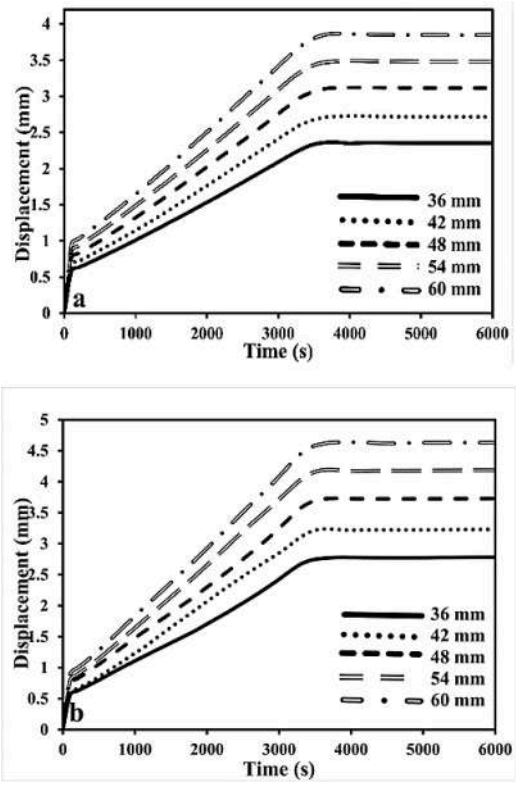

Fig. 11. Effect of coil pitch on actuator displacement during hydriding process in a) $LaNi_5$ granular bed b) $LaNi_5$-Si rubber composite bed (T_o = 295 K, P_o = 5 bar, h = 22 W/m^2 K, Bed thickness = 3 mm, Axial Pitch = 36–60 mm, Spring constant = 10.236–16.535, Coils = 5($LaNi_5$) 8.32 ($LaNi_5$-Si)).

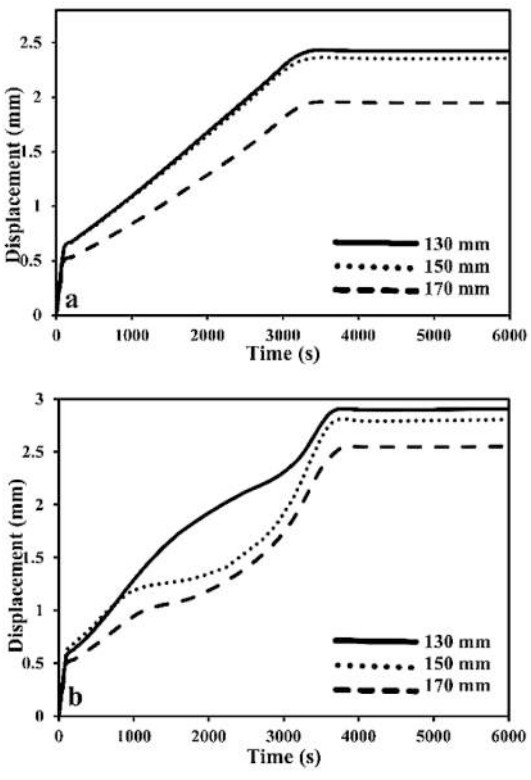

Fig. 12. Effect of coil diameter on actuator displacement during hydriding process in a) $LaNi_5$ granular bed b) $LaNi_5$-Si rubber composite bed (T_o = 295 K, P_o = 5 bar, h = 22 W/m^2 K, Bed thickness = 3 mm, Axial Pitch = 36–60 mm, Spring constant = 10.236–16.535, Coils = 5($LaNi_5$) 8.32 ($LaNi_5$-Si)).

maximum stroke in a shorter time.

The influence of bed thickness respectively on powder and composite actuator attributes is illustrated in Figs. 9 and 10 respectively. The range of values of bed thickness considered were 2.0, 2.5, 3.0 and 3.5 mm. As the thickness increases, in accordance to Fourier's conduction law, the heat transfer rates decrease and the hydrogen absorption process takes longer time to complete. However, owing to larger actuation forces exerted by the larger hydride volume, the actuation stroke is observed to increase with bed thickness. Hence, by increasing bed thickness, the stroke-force properties of the actuator can be increased.

The effect of axial pitch of the spring type hydride-based actuator on the stroke for powder bed case and composite bed case during hydriding process is shown in Fig. 11. With increment in spring pitch, the stroke increases. When the axial pitch increases for a given wire diameter, the shear strength of the spring decreases, resulting in larger actuation stroke.

Fig. 12 gives the variation in axial displacement of the spring for different coil diameters, for the granular and composite beds. As the coil diameter increases, the spring stroke gets altered. For a coiled tube having a certain hydride storage capacity, the axial deflection of the coil decreases with increase in coil diameter. This is due to increase in shear strength imparting more strength to the geometry. For the range of coil diameters undertaken, the stroke of composite actuator shows substantial non-linearities.

The trends in absorption characteristics for the $LaNi_5$-Si rubber composite bed is similar to that of $LaNi_5$ reported in [31,32]. However, the heat transfer rate is comparatively better for the present study. Despite being poor conductors of heat, the incorporation of polymer is momentous in enhancing overall heat conductivity by providing a more efficient path for the heat front to travel compared to the point contact between powder particles. The nature of influence of operational and geometrical parameters are similar to the results obtained in [16].

Conclusions

The main aim of this study is to numerically analyze the performance of a Si rubber polymer dispersed $LaNi_5$ composite actuator for a possible application in soft robotics and haptic interfaces. The purpose of treating the hydride with polymer is to impart better resistance to alloy fragmentation due to cyclic expansion and shrinkage that would otherwise result in low bed thermal conductivity and safety issues to the spring storage. The following conclusions are deduced based on the results obtained:

- From the parallelism in the trends of the concentration and displacement variations for either case, the sorption driven volume expansion is the main contributor to actuation.
- The conductive heat transport rate in the polymer-hydride composite bed is higher.
- The initial response is quick.
- Actuation response to maximum stroke increase with H_2 gas supply pressure and convective heat transfer rates.
- The actuation force increases with thicker beds.
- Trade-off between coil pitch and diameter gives different stroke-force attributes.

In addition to its true purpose of choice, which is to provide stability to the hydride bed during cyclic expansion and contraction, the composite provides enhanced actuation performance. The initial quick response, although in the millimeter scale, can be used as a marker for various sensing parameters. The sorption rate is predominantly controlled by the rate of heat transfer. The scope of incorporating the means to augment the convective heat transfer like using fins or corrugations without inducing stiffness to the geometry can be investigated in the future.

CRediT authorship contribution statement

V. Keshav: Writing – original draft, Visualization, Validation, Software, Methodology, Investigation, Formal analysis. **G. Mohan:** Writing – review & editing, Supervision, Project administration, Conceptualization.

Declaration of competing interest

The authors declare that they have no known competing financial interests or personal relationships that could have appeared to influence the work reported in this paper.

Data availability

Data will be made available on request.

Acknowledgement

This study is supported by All India Council for Technical Education (AICTE) under RPS scheme.

References

[1] A. Khodadadia, S. Gh Liaghata, A.R. Vahid, H.H. Sabet, Ballistic performance of Kevlar fabric impregnated with nanosilica/PEG shear thickening fluid, Compos. B Eng. 162 (2019) 643–652.
[2] S. Zinatloo-Ajabshir, M. Salavati-Niasari, Preparation of magnetically retrievable $CoFe_2O_4$@SiO_2@$Dy_2Ce_2O_7$ nanocomposites as novel photocatalyst for highly efficient degradation of organic contaminants, Compos. B Eng. 174 (2019) 106930.
[3] S. Zinatloo-Ajabshir, M.H. Esfahani, C.A. Marjerrison, J. Greedan, M. Behzad, Enhanced electrochemical hydrogen storage performance of lanthanum zirconium oxide ceramic microstructures synthesized by a simple approach, Ceram. Int. 49 (23 Part A) (2023) 37415–37422.
[4] Malihe Samadi Kazemi, Azam Sobhani, $CuMn_2O_4$/chitosan micro/nanocomposite: green synthesis, methylene blue removal, and study of kinetic adsorption, adsorption isotherm experiments, mechanism and adsorbent capacity, Arab. J. Chem. 16 (2023) 104754.
[5] G. Hosseinzadeh, Seyed Mehdi Sajjadi, Loghman Mostafa, Alireza Yousefi, Reza Hadjiaghaie Vafaie, Sahar Zinatloo-Ajabshir, Synthesis of novel direct Z-scheme heterojunction photocatalyst from WO_3 nanoplates and $SrTiO_3$ nanoparticles with abundant oxygen vacancies, Surf. Interfaces 42 (2023) 103349.
[6] S. Zinatloo-Ajabshir, S. Rakhshani, Z. Mehrabadi, M. Farsadrooh, M. Feizi-Dehnayebi, S. Rakhshani, M. Dušek, V. Eigner, S. Rtimi, T.M. Aminabhavi, Novel rod-like [Cu(phen)2(OAc)]·PF6 complex for high-performance visible-light-driven photocatalytic degradation of hazardous organic dyes: DFT approach, Hirshfeld and fingerprint plot analysis, J. Environ. Manage. 350 (2024) 119545.
[7] George M. Lloyd, Kwang J. Kim, Smart hydrogen/metal hydride actuator, Int. J. Hydrogen Energy 32 (2007) 247–255.
[8] Kwangmok Jung and Kwang J. Kim, A thermokinetically driven metal-hydride actuator, in: Proceedings of SPIE, Vol.6932, Sensors and Smart Structures Technologies for Civil, Mechanical and Aerospace Systems, 2008.
[9] Minako Hosono, Shuichi Ino, Mitsuru Sato, Kazuhiko Yamashita, Takashi Izumi, A system utilizing metal hydride actuators to achieve passive motion of toe joints for prevention of pressure ulcers: a pilot study, Rehab. Res. Practice (2012).
[10] S. Ino, M. Sato, M. Hosono, T. Izumi, Development of a soft metal hydride actuator using a laminate bellows for rehabilitation systems, Sens. Actuators B 136 (2009) 86–91.
[11] Y. Nishi, H. Uchida, H. Yabe, B. Kim, T. Ogasawara, Giant bending motion of a soft actuator controlled by hydrogen gas pressure, J. Intell. Mater. Syst. Struct. 17 (8) (2006) 709–711.
[12] M. Mizumoto, T. Ohgai, A. Kagawa, Bending behavior of Cu-plated Pd-Ni alloy ribbon driven by hydrogenation, J. Alloy. Compd. 482 (2009) 416–419.
[13] A. Nakai, M. Mizumoto, A. Kagawa, Bending and rotation movement control of a novel actuator utilizing hydrogen storage alloys, Adv. Mat. Res. 156–157 (2011) 1170–1175.
[14] K. Numasaki, T. Honjoh, H. Uchida, Y. Matsumura, Y. Nishi, High responsive unimorph actuator of $LaNi_5$ hydrogen storage alloy film deposited on polyimide sheet, Smart Materials III, Proceeding of SPIE 5648 (2005).
[15] K. Goto, T. Hirata, T. Higuchi, O. Fuchiwaki, S. Ozaki, W. Nakao, Deformation mechanism of capsule-type hydrogen-storage-alloy actuator, Int. J. Hydrogen Energy 44 (2019) 16877–16886.
[16] P.V. Jithu, G. Mohan, Performance simulation of metal hydride based helical spring actuators during hydrogen sorption, Int. J. Hydrogen Energy 47 (33I) (2022) 14942–14951.
[17] H. Uchida, T. Ebisawa, K. Terao, N. Hosoda, Y.C. Huang, Hydriding and dehydriding characteristics of $LaNi_5$ mixed with silicone compounds, J. Less-Common Met. 131 (1987) 365–369.

[18] P.R. Bidez, A.J. Goudy, A. Zarynow, Hydriding and dehydriding kinetics of $LaNi_5$ mixed with silicone rubber, Micromech. J. 47 (1993) 108–114.
[19] M. Pentimalli, A. Frazzica, A. Freni, E. Imperi, F. Padella, Metal hydride-based composite materials with improved thermal conductivity and dimensional stability properties, Adv. Sci. Technol. 72 (2010) 170–175.
[20] R. Checchetto, N. Bazzanella, A. Miotello, G. Carotenuto, Synthesis and characterization of polymer embedded LaNi5 composite material for hydrogen storage, J. Phys. D Appl. Phys. 40 (2007) 4043–4048.
[21] R. Checchetto, N. Bazzanella, A. Miotello, G. Carotenuto, L. Nicolais, Hydrogen sorption in metal-polymer composites: the role of interfaces, J. Appl. Phys. 105 (2009) 083513(1)–083513(6).
[22] W.R. Schmidt, Hydrogen storage in polymer-dispersed metal hydrides. Proceedings of the 2001 DOE Hydrogen Program Review NREL/CP-570-30535, 2001.
[23] Hu. Xiaochen, Z. Qi, F. Qin, J. Chen, Mechanism analysis on stress accumulation in cylindrical vertical-placed metal hydride reactor, Energy Power Eng. 334059 (04) (2011) 490–498.
[24] K. Pietrak, T.S. Wiśnieswski, A review of models for effective thermal conductivity of composite materials, J. Power Technol. 95 (1) (2005) 14–24.
[25] C. Briki, P. de Rango, S. Belkhiria, Mohamed Houcine Dhaou, Abdelmajid Jemni, Measurements of expansion of $LaNi_5$ compacted powder during hydrogen absorption/desorption cycles and their influences on the reactor wall, Int. J. Hydrogen Energy 44 (26) (2019) 13647–13654.
[26] M. Moawed, Experimental investigation of natural convection from vertical and horizontal helicoidal pipes in HVAC applications, Energ. Conver. Manage. 46 (2005) 2996–3013.
[27] K.K. Phani, S.K. Niyogi, Youngs modulus of porous brittle solids, J. Mater. Sci. 22 (1987) 257–263.
[28] G. Lekshmi Dinachandran, Mohan, Numerical simulation of the parametric influence on the wall strain distribution of vertically placed metal hydride based hydrogen storage container, Int. J. Hydrogen Energy 40 (16) (2015) 5689–5700.
[29] K. Makarian, S. Santhanam, Z.N. Wing, Coefficient of thermal expansion of particulate composites with ceramic inclusions, Ceram. Int. 42 (15) (2016) 17659–17665.
[30] AZoM.com – An AZoNetwork Site (2022) Properties: Silicone Rubber (azom.com).
[31] G. Mohan, M. Prakash Maiya, S. Srinivasa Murthy, Performance of air cooled hydrogen storage device with external fins, Int. J. Low Carbon Technol. 3 (4) (2008).
[32] G. Mohan, M. Prakash Maiya, S. Srinivasa Murthy, Performance simulation of metal hydride hydrogen storage device with embedded filters and heat exchanger tubes, Int. J. Hydrogen Energy 32 (2007) 4978.